5.3.5 Solid Dispersion Modelling

The ability to predict solids concentration in the slurry along the axis of the column is important. This will enable us to compute the average concentration in the column, which could be important in determining factors that affect the coal reactions occurring in the dissolver.

Figure 120. **EFFECT OF DISTRIBUTOR ON NORMALIZED SOLIDS DISTRIBUTION**

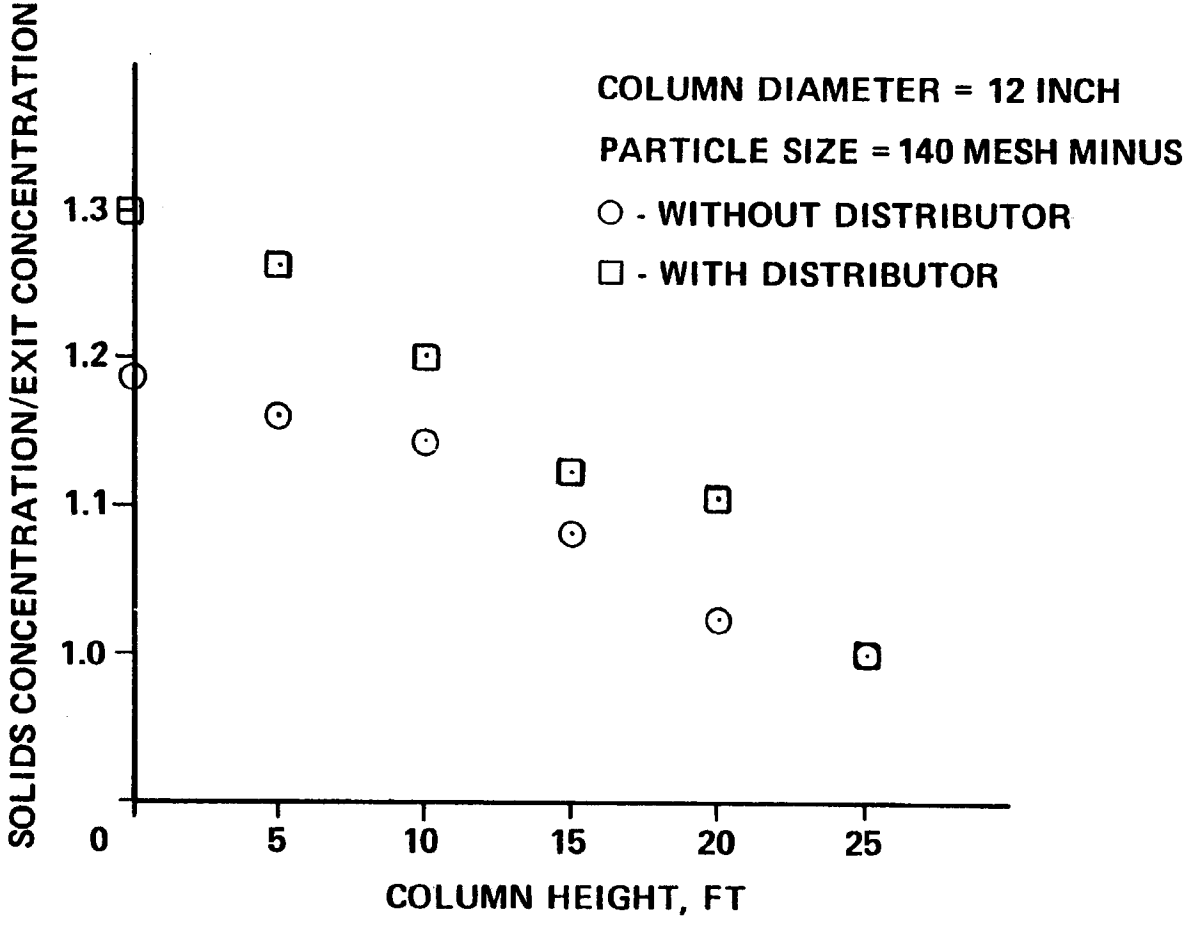

Figure 121

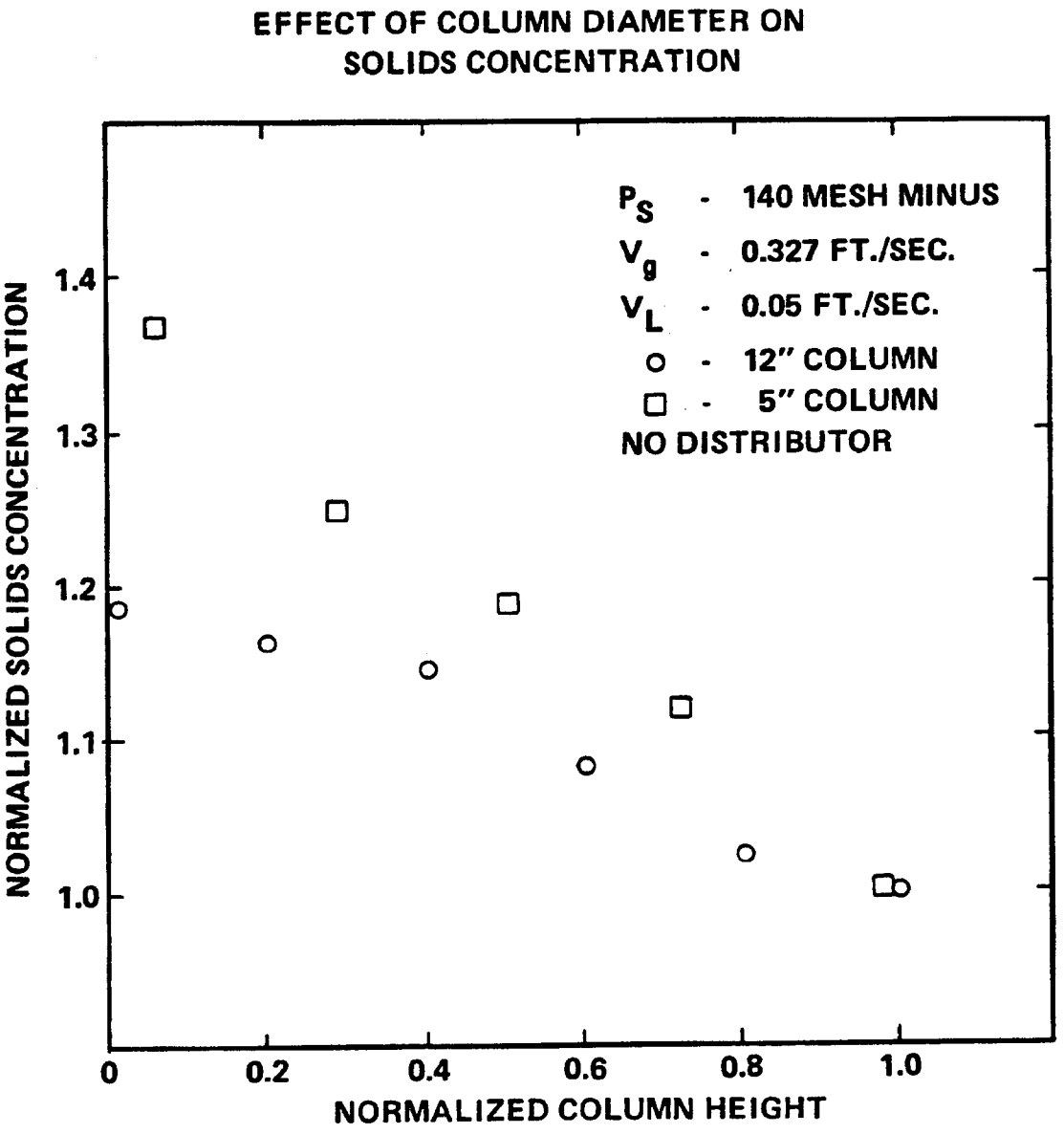
EFFECT OF COLUMN DIAMETER ON
SOLIDS CONCENTRATION
P_S - 140 MESH MINUS
V_g - 0.327 FT./SEC.
V_L - 0.05 FT./SEC.
○ - 12" COLUMN
□ - 5" COLUMN
NO DISTRIBUTOR
NORMALIZED SOLIDS CONCENTRATION
1.4
1.3
1.2
1.1
1.0
0
0.2
0.4
0.6
0.8
1.0
NORMALIZED COLUMN HEIGHT

Figure 122

Effect of Column Diameter

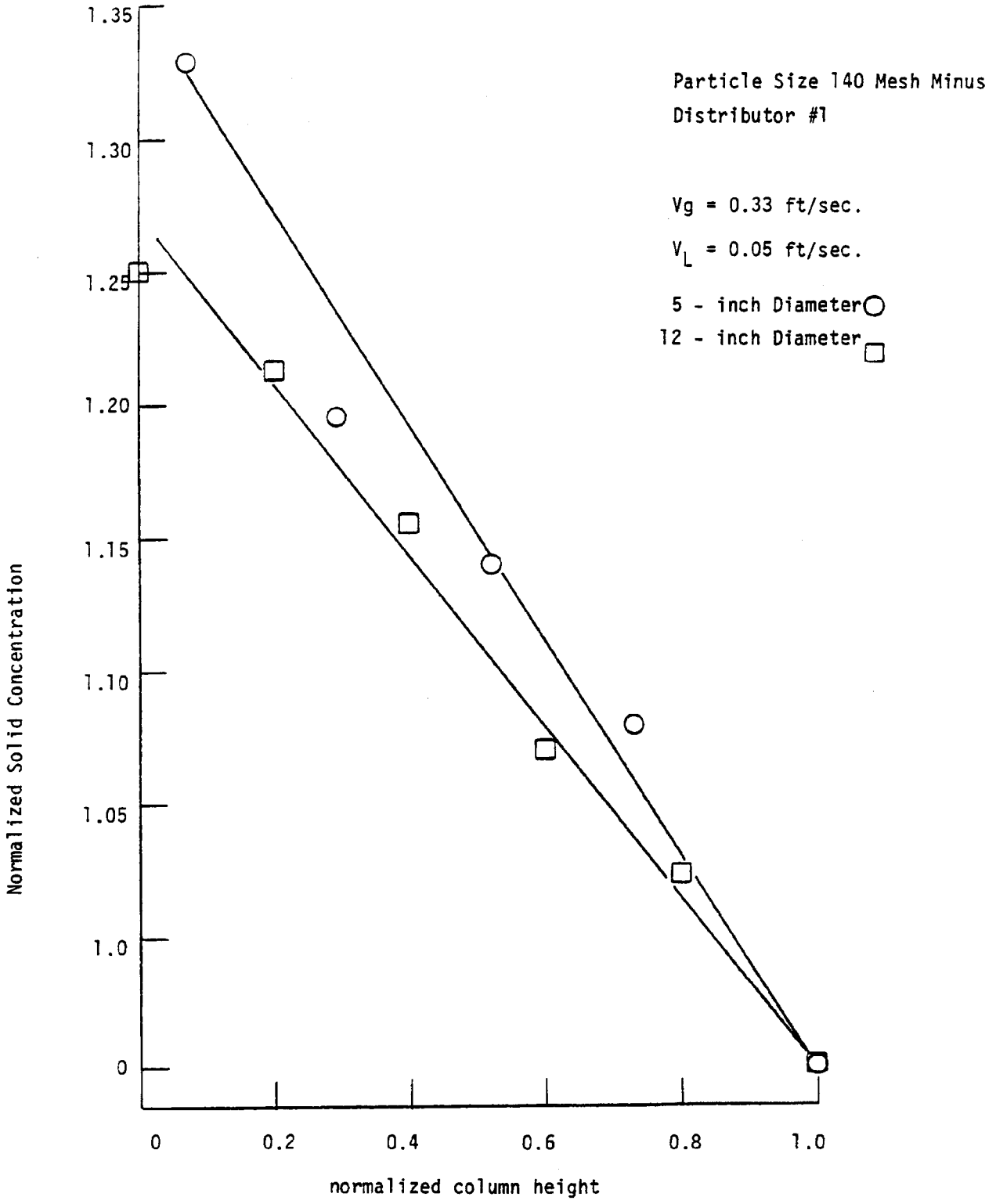

Based on a one-dimensional axial solids dispersion model that assumes steady-state conditions, our model is essentially a mass balance of the solid particles at any cross section. The equation is as follows:

$$\frac{u_\ell}{1 - \varepsilon_g} (C - C_f) - E_{zp} \frac{dC}{dL} - V_p C = 0 \qquad (6)$$

where u_ℓ = superficial liquid velocity (ft/sec); ε_g = average gas holdup; C = axial solids concentration in slurry (lbm/ft^3); C_f = feed slurry concentration (lbm/ft^3); E_{zp} = axial solids dispersion coefficient (ft^2/sec); L = axial height (ft); V_p = particle settling velocity (ft/sec).

Rearranging equation (6) by dividing by E_{zp} gives:

$$\frac{u_\ell}{E_{zp}(1 - \varepsilon_g)}(C - C_f) - \frac{dC}{dL} - \frac{V_p}{E_{zp}} C = 0 \qquad (7)$$

The values of u_ℓ, E_{zp}, C_f and V_p/E_{zp} are required for this model.

From the earlier section (5.3.3) on solids dispersion we obtained values of V_p/E_{zp} for different gas velocities and different average solids concentrations. Usually, V_p/E_{zp} decreased as the average concentration of solids in the column increased. This was attributed to a decrease in V_p as the concentration increased.

No direct means were used to measure E_{zp}, but we assumed that:

$$E_{zp} = E_{zl} \text{ (liquid dispersion coefficient)} \qquad (8)$$

The basis for this assumption is that the particles still follow the movements of the liquid fluctuations to a reasonable degree. Also, another assumption that was made was that $V_p/E_{zp} = V_p/E_{zp}$ (c), i.e. function of local concentration. Hence this ratio will vary with column height. The value of E_{zl} was already obtained in experiments described previously in the liquid dispersion section (5.2).

Due to the possibility of random erros in the measurement of the feed concentration (C_F) the C_F value used in this model was optimized to provide the best agreement between the integrated experimental data and the calculated area of the model profile. We used an iterative method that was usually fast; on the average, about 13 iterations were required to attain a relative accuracy of 10^{-4}; i.e.;

$$\frac{W_{Calcd} - W_{act.}}{W_{act}} \leq 10^{-4} \qquad (9)$$

where $W_{cald.}$ and $W_{act.}$ are amounts of solids retained in the column by calculation and actual measurement, respectively.

Figures D1 to D40 in Appendix D plot the results of 40 runs conducted in water, tetralin, 50% glycol in the 12-in. diameter column and compare these data with the model. All of these data except for two runs with 60/80 mesh sand in 50% glycol showed good agreement between the model and experimental results. In the two runs that did not agree, mixing above the distributor plate was poor due to the low gas velocity employed (V_g = 0.05 ft/sec).

Hence, the one-dimensional model shows good agreement with experimental data. It also reveals that a liquid axial dispersion coefficient can be used instead of a solid dispersion coefficient, at least for particles as large as 60/80-mesh sand. In addition, the assumption that exit concentration is reasonably close to the feed concentration seems to be correct as seen by the C_F values predicted by the model.

5.4 Gas/Liquid Mass Transfer

Gas/liquid mass-transfer rates in both air/water and air/water/sand systems were investigated in the 5-in. and 12-in. diameter columns. The mass-transfer coefficient was determined from the rate at which oxygen is transferred from air to water during batch-mode operation (no liquid flow). This method has been used by other investigators and was described in detail in the Experimental Section.

The gas/liquid mass-transfer coefficient ($k_L a$) was calculated by assuming that the system was completely backmixed:

$$k_L a = \frac{1 - \varepsilon_g}{t} \ln \frac{C^* - C_i}{C^* - C_f} \qquad (10)$$

where $k_L a$ = volumetric liquid-phase mass-transfer coefficient, (sec^{-1}); ε_g = gas volume fraction (or gas holdup); t = time (sec); C^* = equilibrium oxygen concentration (mg/ℓ); C_i = initial concentration of dissolved oxygen (mg/ℓ); C_f = final concentration of dissolved oxygen (mg/ℓ).

Our liquid dispersion results show that we can validly assume that the liquid phase is completely backmixed. Comparing our liquid dispersion results with a tank-in-series model indicated that the simulator columns (5-in. and 12-in. diameters) closely resemble 1.1 stirred tank in series, this supports the validity of the simple backmixed assumption used to calculate the gas/liquid mass-transfer coefficient.

5.4.1 Gas/Liquid Two-Phase System

The gas/liquid mass transfer coefficient, $k_L a$, increases with increasing gas velocity. The increase in $k_L a$ is largely due to the increase of gas/liquid interfacial contact as gas velocity increases. The mass-transfer coefficients measured in the 5-in.-diameter column were the

same as predictions from the correlation of Yoshida and Akita (12) (Figure 123). This agreement further supports the experimental technique we used to measure the mass-transfer coefficient. Yoshida and Akita's correlation includes the physical properties of the liquid phase and the diameter of the bubble column in several dimensionless groups, as shown by:

$$N_{Sh}(aD) = C_1 N_{Sc}^{0.5} N_{Bo}^{0.62} N_{Ga}^{0.31} \varepsilon_g^{1.1} \qquad (11)$$

where N_{Sh} = the Sherwood number = $k_L D/D_L$ (dimensionless); a = specific gas/liquid interfacial area (L^{-1}); D = column diameter (L); C_1 = dimensionless constant; N_{Sc} = Schmidt number = υ_L/D_L (dimensionless); N_{Bo} = Bond Number = $gD^2\rho_L/\gamma$ (dimensionless); N_{Ga} = Galileo number = gD^3/υ_L^2 (dimensionless); ε_g = gas holdup (dimensionless); k_L = liquid-phase mass transfer coefficient (LT^{-1}); D_L = liquid-phase diffusivity (L^2T^{-1}); υ_L = liquid-phase kinematic viscosity (L^2T^{-1}); g = gravitational constant (LT^{-2}); ρ_L = liquid density (ML^{-3}); γ = surface tension (MT^{-2}).

Hence the agreement shown in Figure 123 also suggests the possible application of this correlation to the SRC-I coal system and scale up to industrial size.

Our results indicate that the gas/liquid mass-transfer rate is independent of column position; the rate is the same at the bottom as at the top of the column. That the rate does not depend on column position is not surprising, because the liquid phase is practically completely backmixed. Since the mass transfer rate is calculated from the oxygen uptake in the bulk liquid, one should not anticipate any effect of column position. Results from experiments with the 12-in. diameter column further substantiate this.

Although the gas/liquid mass-transfer coefficients measured in the 12-in.-diameter column increase as gas velocity increases the values deviate from Yoshida and Akita's correlation at high gas velocities, as shown in Figure 124. The measured values were always lower than

Figure 123

Effect of Solids on Gas/Liquid Mass Transfer Coefficient

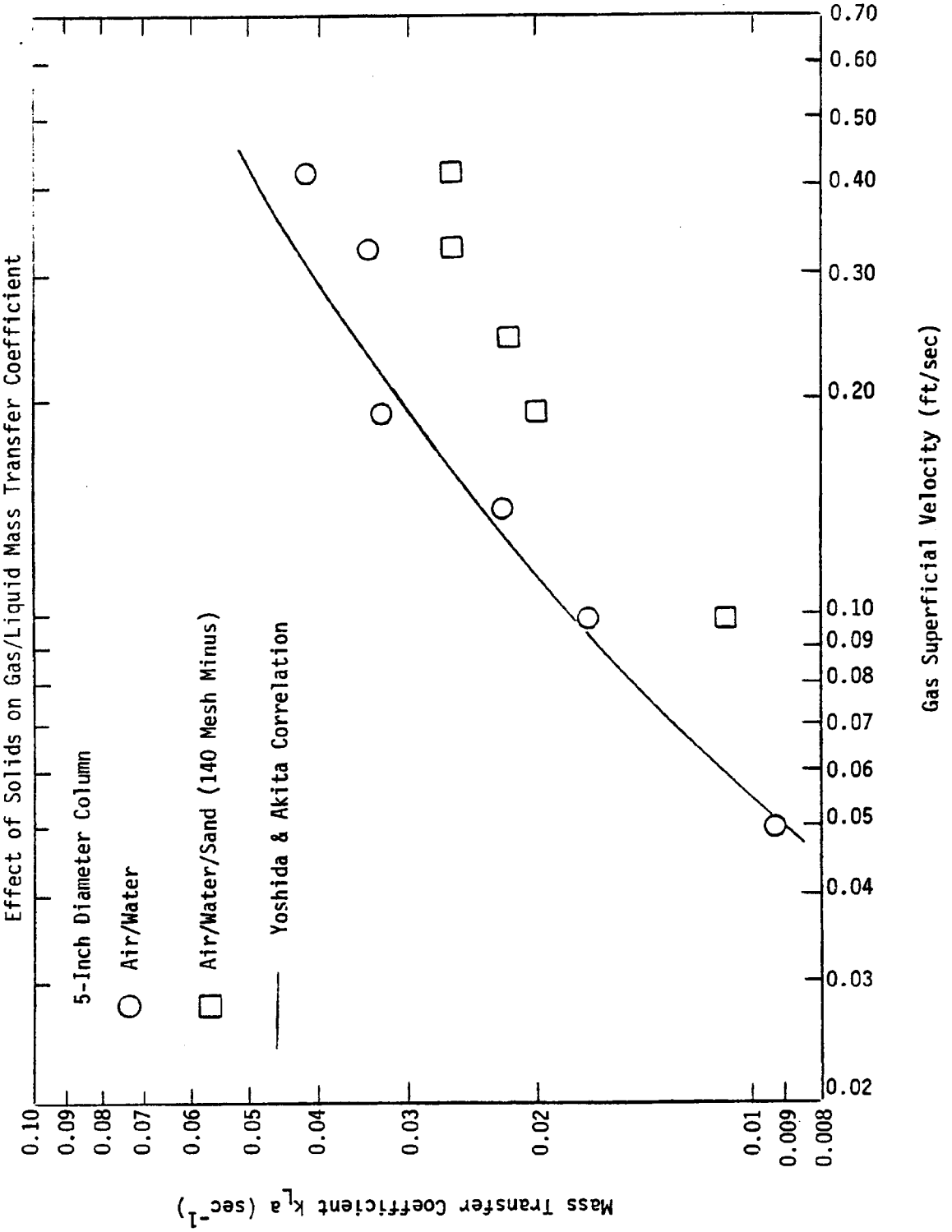

FIGURE 124
GAS/LIQUID MASS TRANSFER IN A 12-INCH DIAMETER COLUMN

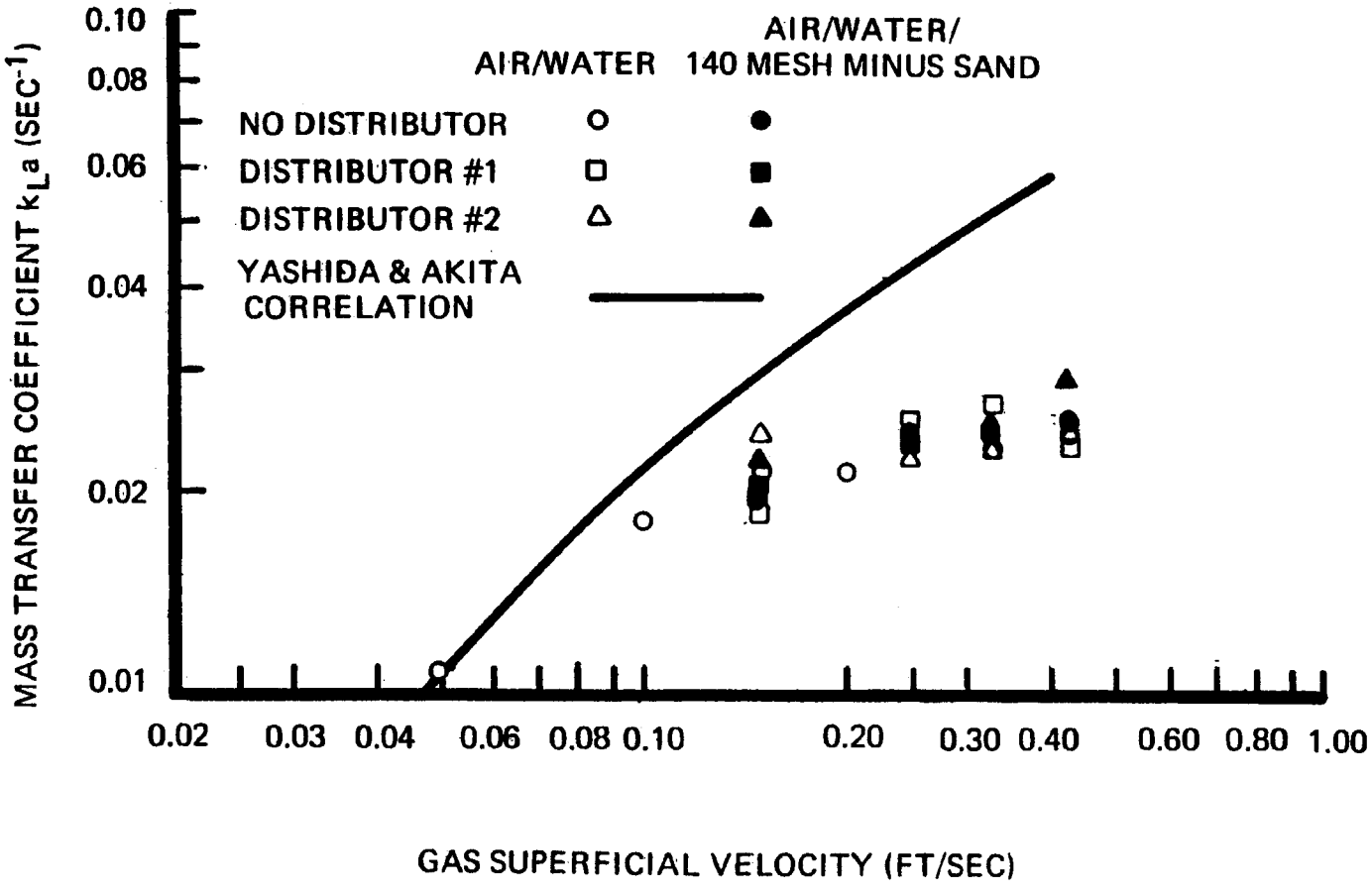

those predicted. One possible explanation is the high L/D ratio of the 12-in. column. As observed in the gas holdup study, the fraction of large bubbles in the 12-in. column is substantial and increases with increasing gas velocity. An increased fraction of large bubbles means gas/liquid interfacial contact is reduced. Since the k_La value increases with increasing gas velocity because of more gas/liquid interfacial contact, the fraction of large gas bubbles observed in the 12-in. diameter column, which has a high L/D ratio, reasonably explains the deviation shown in Figure 124. This finding raises an important point. Because Yoshida and Akita's correlation was developed using a low L/D ratio column, correction is required if a high L/D ratio column is used.

In addition, the distributor plate does not affect the gas/liquid mass-transfer rate. Within experimental accuracy, the k_La values measured without a distributor plate and with two different distributor designs are the same as shown in Figure 124. The entrance effect is usually limited to a distance of a few diameters above the distributor plate. Therefore, it is not surprising that the mass-transfer rate is independent of entrance effect in the high L/D ratio column.

5.4.2 Gas/Liquid/Solid Three-Phase System

The presence of solids (-140 mesh sand) reduces the gas/liquid mass-transfer rate measured in an air/water system in the 5-in.-diameter column (Figure 123). The average bubble size in any bubble column resulted from the balance of bubble coalescence and break-up rates. The work of Kato et al. (4) showed that solids enhances the bubble coalescence rate, resulting in larger gas bubbles. Thus, gas/liquid interfacial contact will decrease, which qualitatively explains the reduction in the mass-transfer coefficient we observed.

However, the effect of solid particles is less apparent in the 12-in. column. The k_La values for the same system are indistinguishable from those for the air/water system (see Figure 124). Perhaps the substantial fraction of large gas bubbles that exist in a high L/D

ratio column (as discussed earlier) reduces the effectiveness of the solid particles in enhancing bubble coalescence rate. This qualitative explanation seems logical, but more work is needed to understand mass transfer in a three-phase system. In any event, the lower $k_L a$ values observed in the 5-in. column suggest that Yoshida and Akita's correlation must be modified to account for the effect of solids.

At this stage, our results are insufficient to make any detailed modifications. However, an empirical correction can be obtained by reducing the dimensionless constant (C_1) in equation 1 from 0.60 to 0.36. Figure 125 compares this empirically modified expression with the $k_L a$ values determined for the air/water/sand system in the 5-in. column. The agreement shown in Figure 125 suggests the possible application of this modified correlation to determine the effect of solids. Nonetheless, more work is needed either to test this correlation or to develop an expression for three-phase system.

FIGURE 125
GAS/LIQUID MASS TRANSFER IN A 5-INCH DIAMETER COLUMN

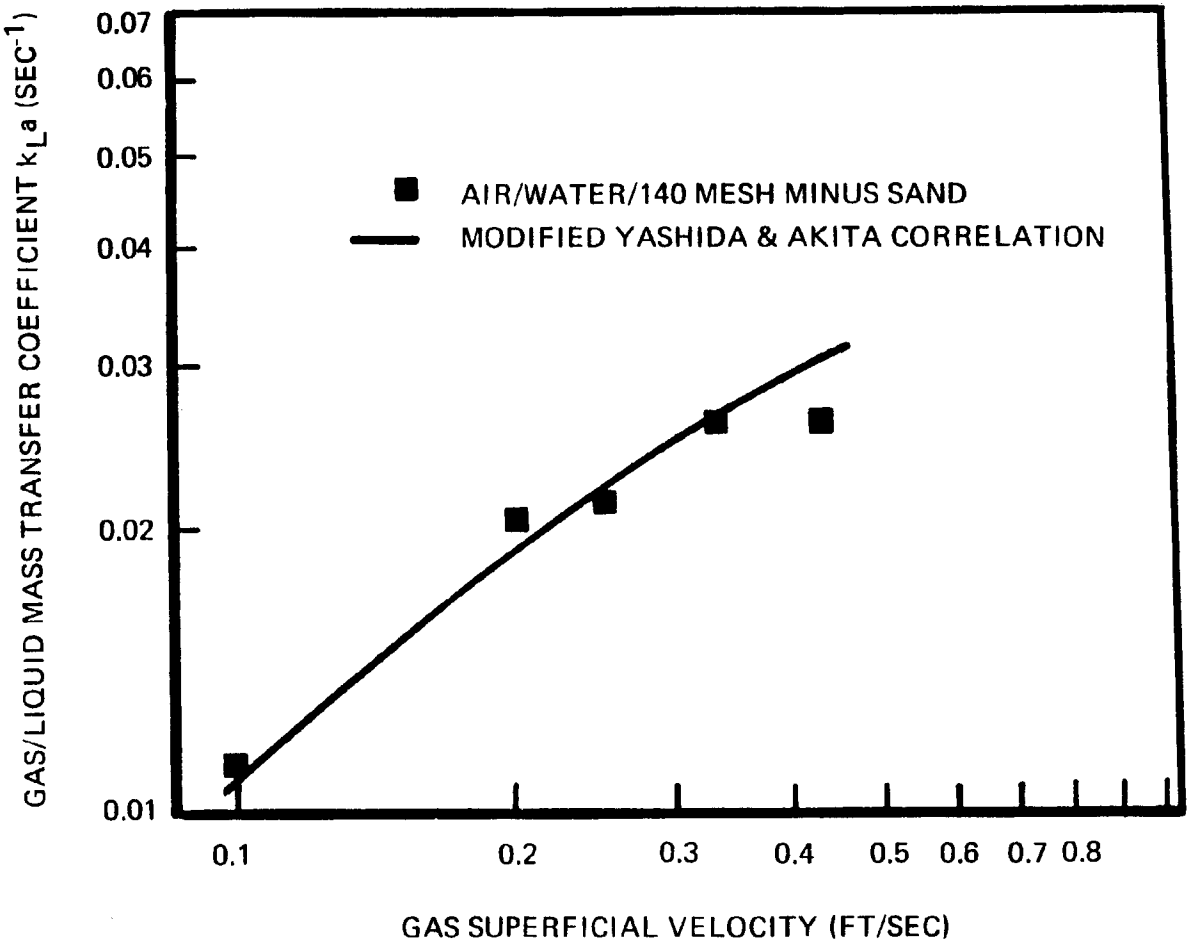

5.5 Solids Removal

Solids removal experiments were also conducted both in the 5-in. and 12-in.-diameter columns, to test the effectiveness of slurry withdrawal from the column bottom to control solids accumulation. Most of the experiments were terminated before a steady-state solid distribution profile was reached. However, some preliminary conclusions can be drawn from the available data.

The results clearly indicate that withdrawing solids at the reactor bottom significantly reduces solids accumulation and changes the concentration profile of the solids retained in the column. Results from the 5-in. column experiments are plotted in Figures 126 and 127. Figure 126 shows the data for 60/80 mesh solids, obtained at various column heights as a function of time. In the beginning of the experiment, a sand/water slurry was allowed to recycle through the column until steady state was obtained. Sampling after 90 and 120 min. of operation clearly indicated that a steady-state condition was reached. At 130 min. the bottom sample port was opened to start the solid withdrawal test; simultaneously, the recycle mode of operation was changed to a once-through mode. The average rate of slurry withdrawal was about 15% of the slurry volumetric feed rate. Slurry samples were obtained along the column at various durations after the start of the withdrawal run.

The results Figure 126 indicate that the solid concentration at every column position decreased after the start of solid withdrawal. Figure 127 presents the solid concentration profile reduced from the data shown in Figure 126. After 36 min. of solids withdrawal, the amount of retained solids decreased by 50%. Using solids concentration profiles shown in Figure 127, we calculated the amount of retained solids in the column. Figure 128, which plots the retained solids as a function of withdrawal time, clearly illustrates that the amount of solids retained decreases with increasing operating time. However, a steady-state value was not reached at the end of the experiment. In addition, the concentration profile changes drastically, as illustrated in Figure 127.

Figure 126. **EFFECT OF SOLIDS WITHDRAWAL ON SOLIDS DISTRIBUTION**

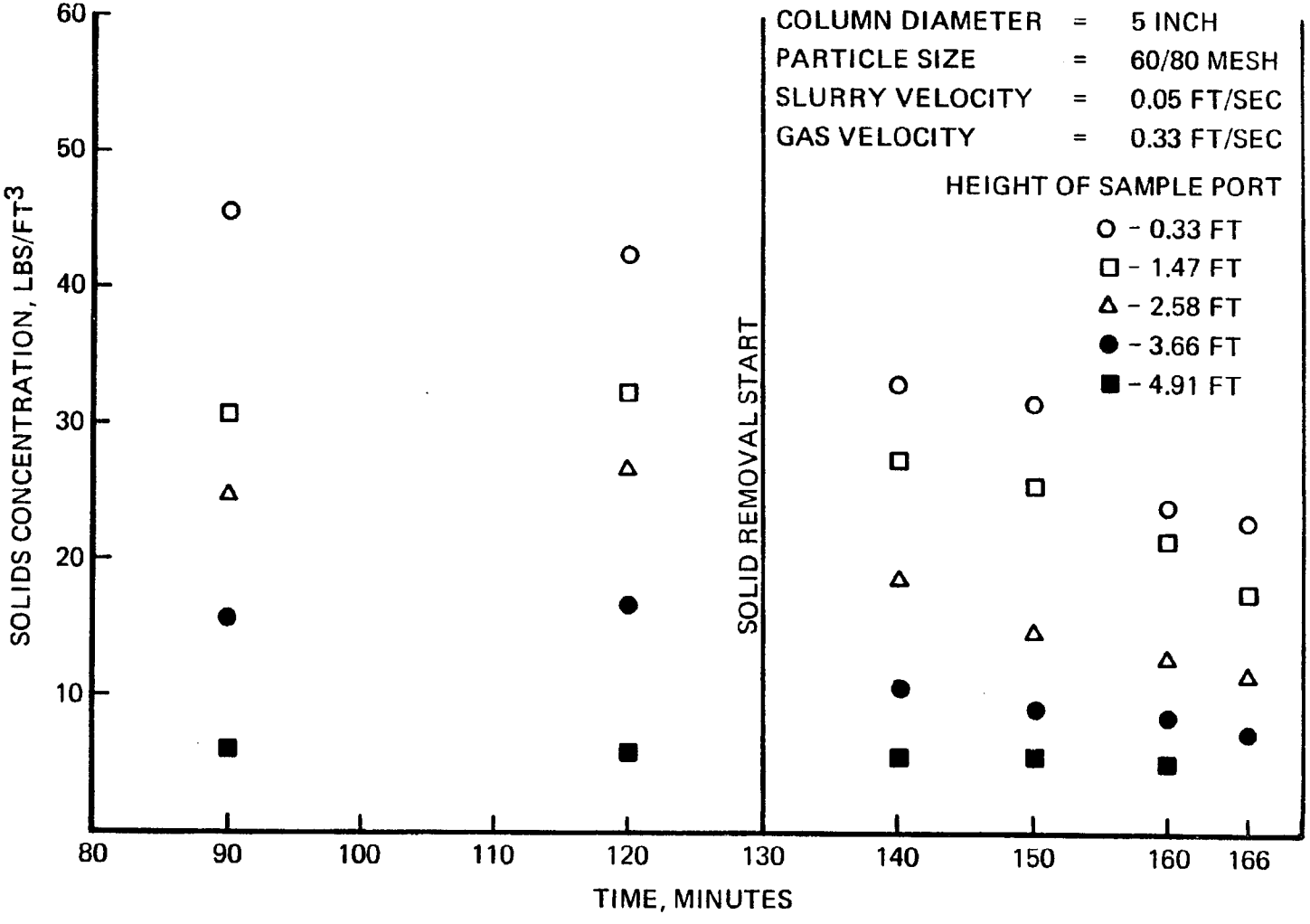

Figure 127. **EFFECT OF SOLIDS WITHDRAWAL ON AXIAL SOLIDS DISTRIBUTION**

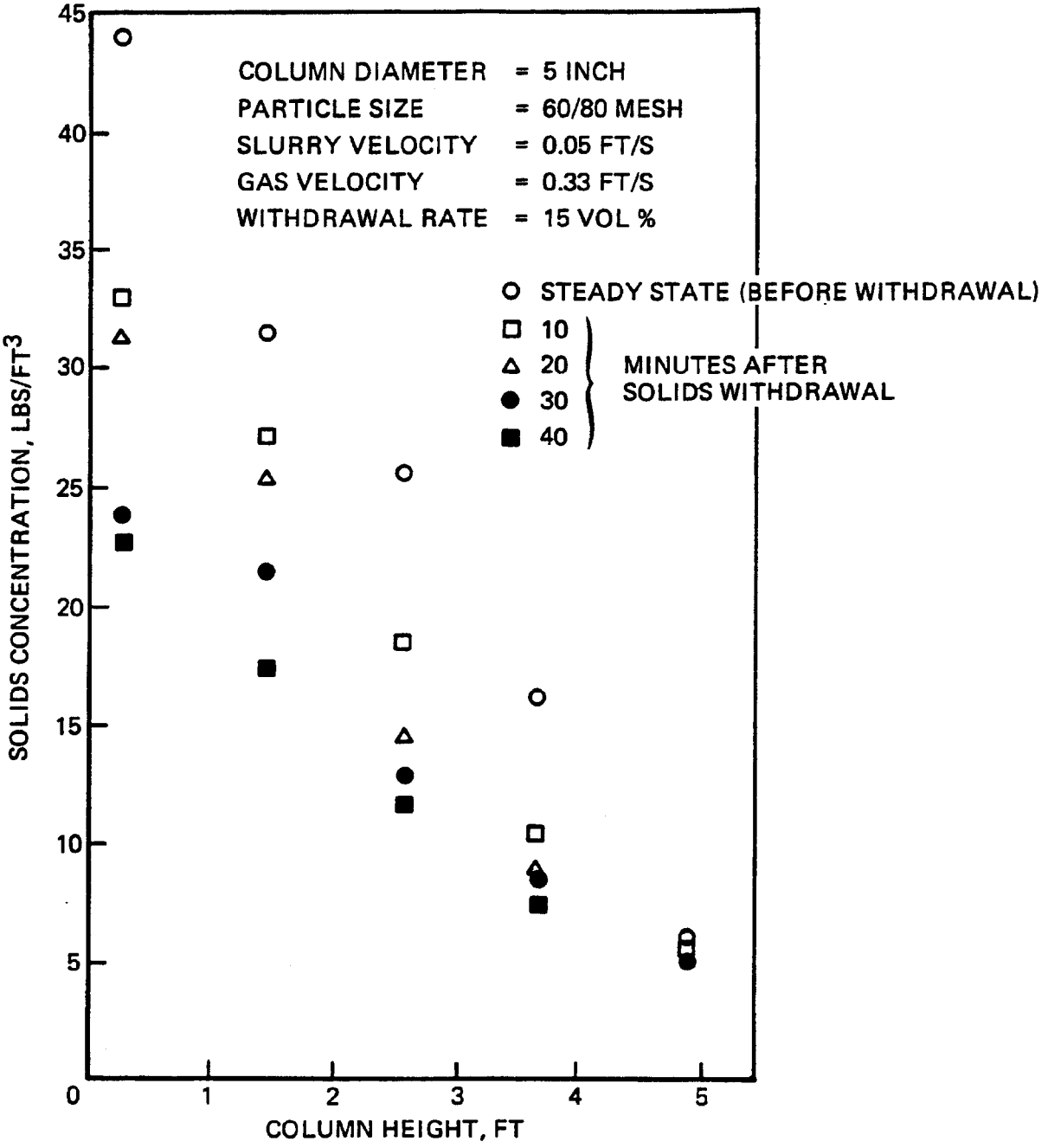

Figure 128.

EFFECT OF SOLIDS WITHDRAWAL TIME ON RETAINED SOLIDS

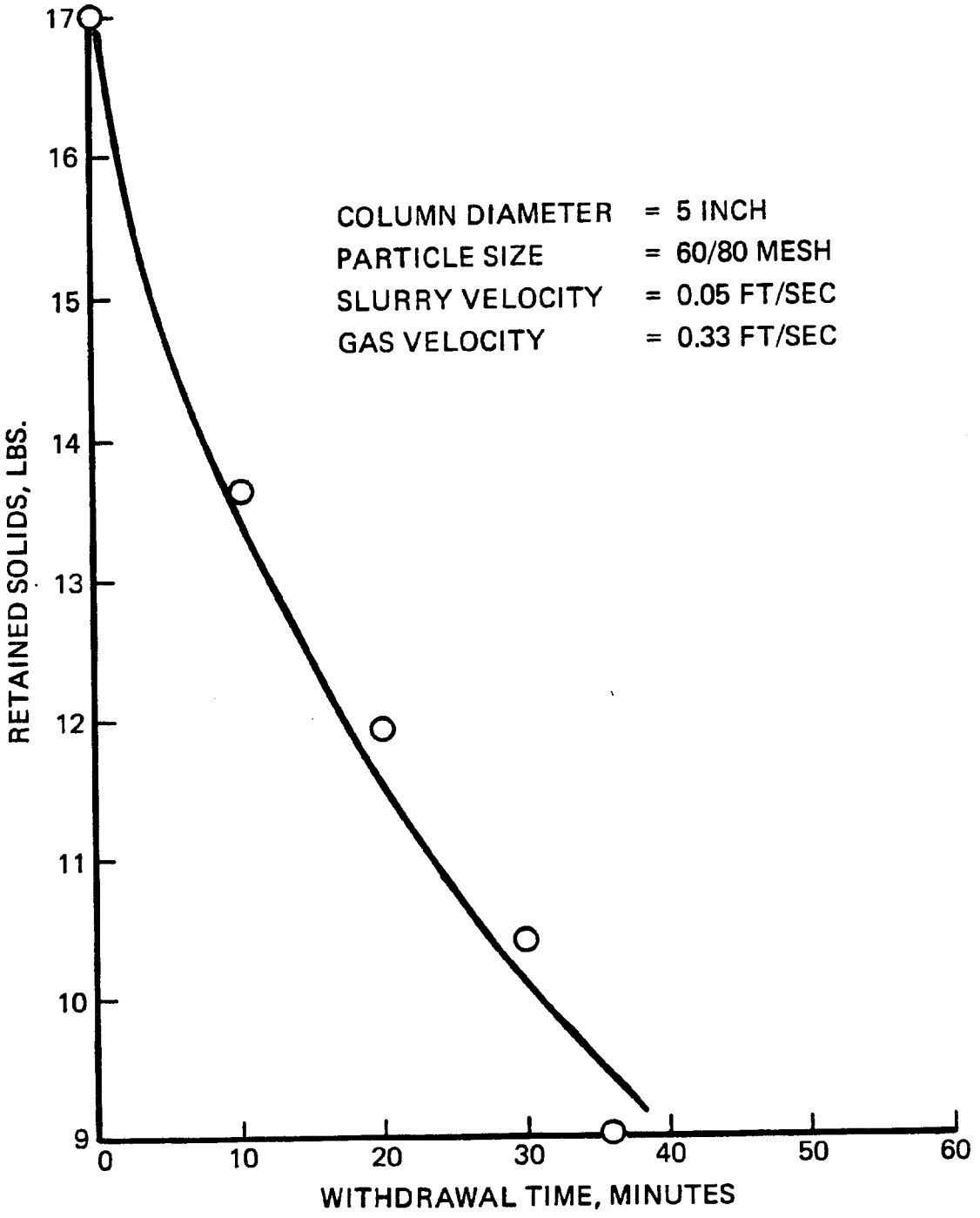

The withdrawal rate has a significant impact on the amount of solids retained in the column. Results from experiments conducted in the 12-in. column using 60/80 mesh particles at different withdrawal rates are graphed in Figures 129 through 131 because precise control of the withdrawal rate was difficult and the rate varies in each experiment. At a low withdrawal rate (varied between 6 and 9% of the volumetric slurry feed rate), solids removal did not seem to affect the solids concentration at all positions along the column axis within the experimental time frame. In this experiment, the solids withdrawal rate was unsteady because the withdrawal line clogged frequently.

However, at higher withdrawal rates, solids removal definitely changed the distribution profile. Figures 130 and 131 show the results at withdrawal rates of 23-29 and 20-22%, respectively. The concentration profile in the column is significantly affected at high withdrawal rates, compared to the results obtained at low rates. Again, steady-state values were not reached in this short experiment. But the sharp difference in the non-steady-state concentration profiles at low and high removal rates definitely suggests the strong impact of the rate of solids withdrawal on solids accumulation.

An experiment with both 20/30 and 60/80 mesh sand showed that the solids withdrawal system located at the bottom of the column preferentially removed larger particle. In this experiment a known amount of 20/30 mesh sand particles was placed in the column, and a slurry containing 60/80 mesh particles was recycled through the column. Two steady-state samples were withdrawn from all the sample ports, and three samples were taken after the start of solids withdrawal. Figure 132 graphs the solids concentration at various axial positions in the column as a function of time, and Figure 133 shows the axial solids distribution before and after solids withdrawal. Both figures indicate clearly that solids distribution changes when withdrawal is employed and fewer solids are retained.

Figure 129. **EFFECT OF SOLIDS WITHDRAWAL ON SOLIDS DISTRIBUTION**

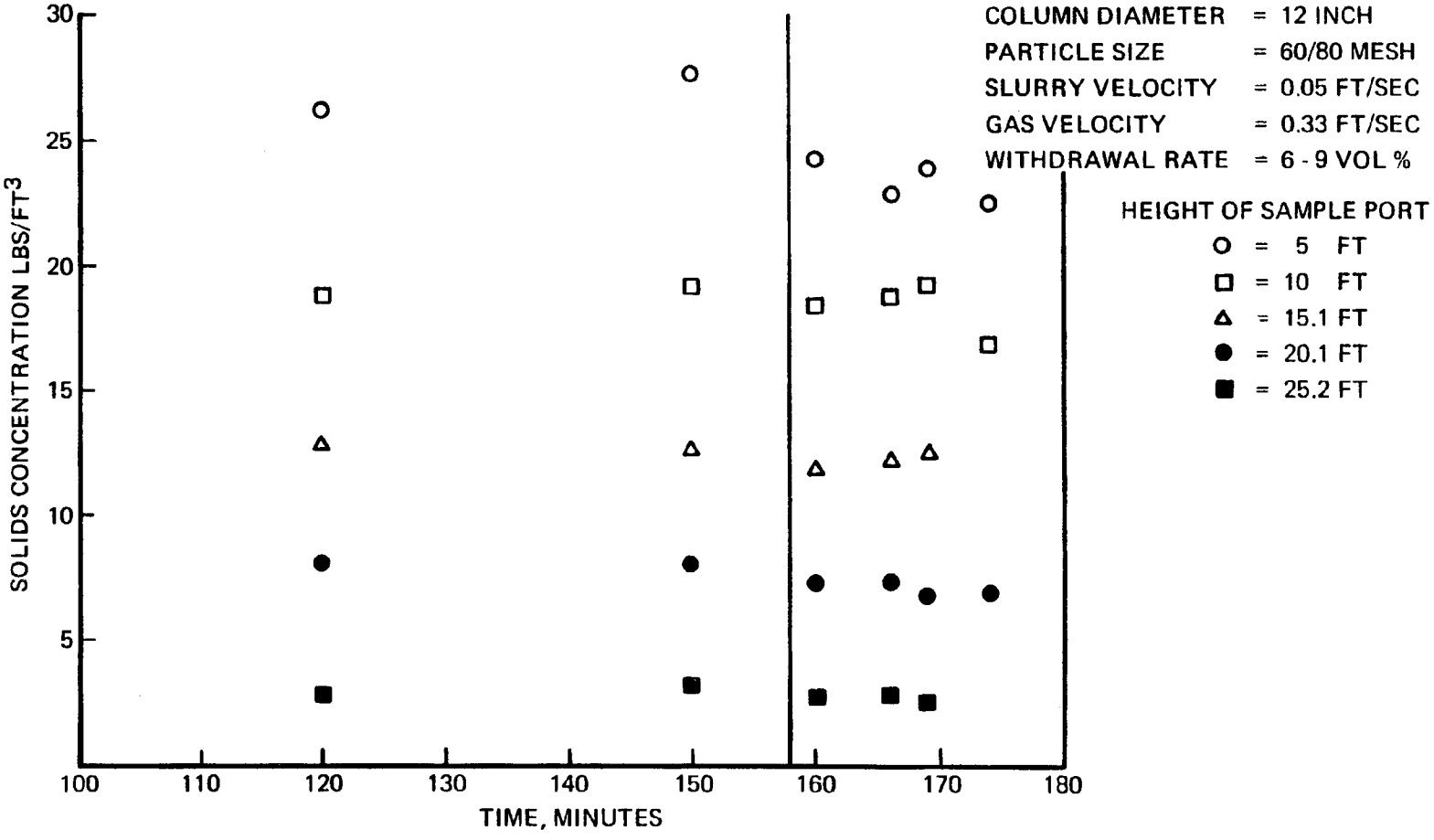

Figure 130. **EFFECT OF SOLIDS WITHDRAWAL ON SOLIDS DISTRIBUTION**

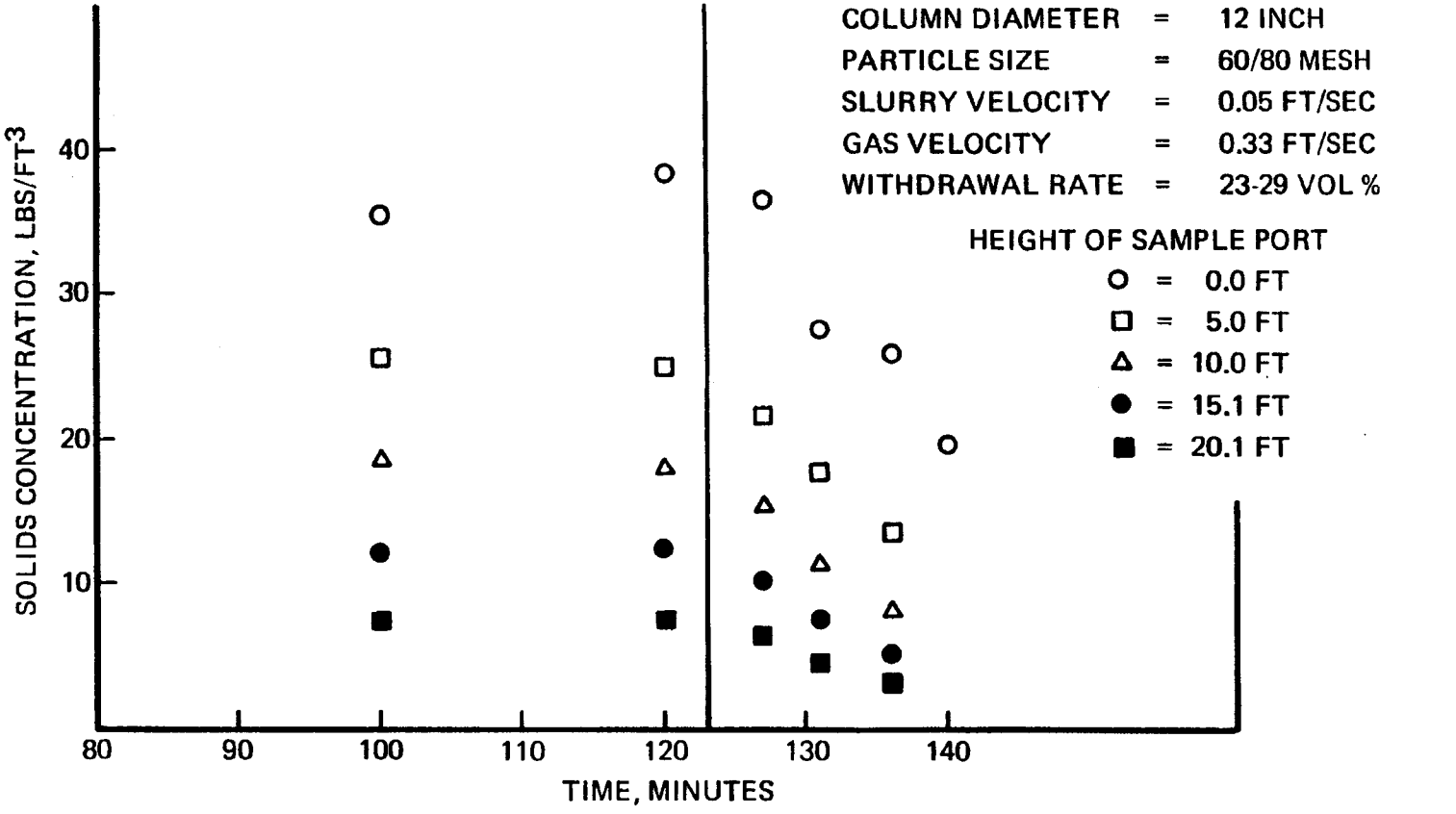

Figure 131

EFFECT OF SOLIDS WITHDRAWAL ON SOLIDS DISTRIBUTION

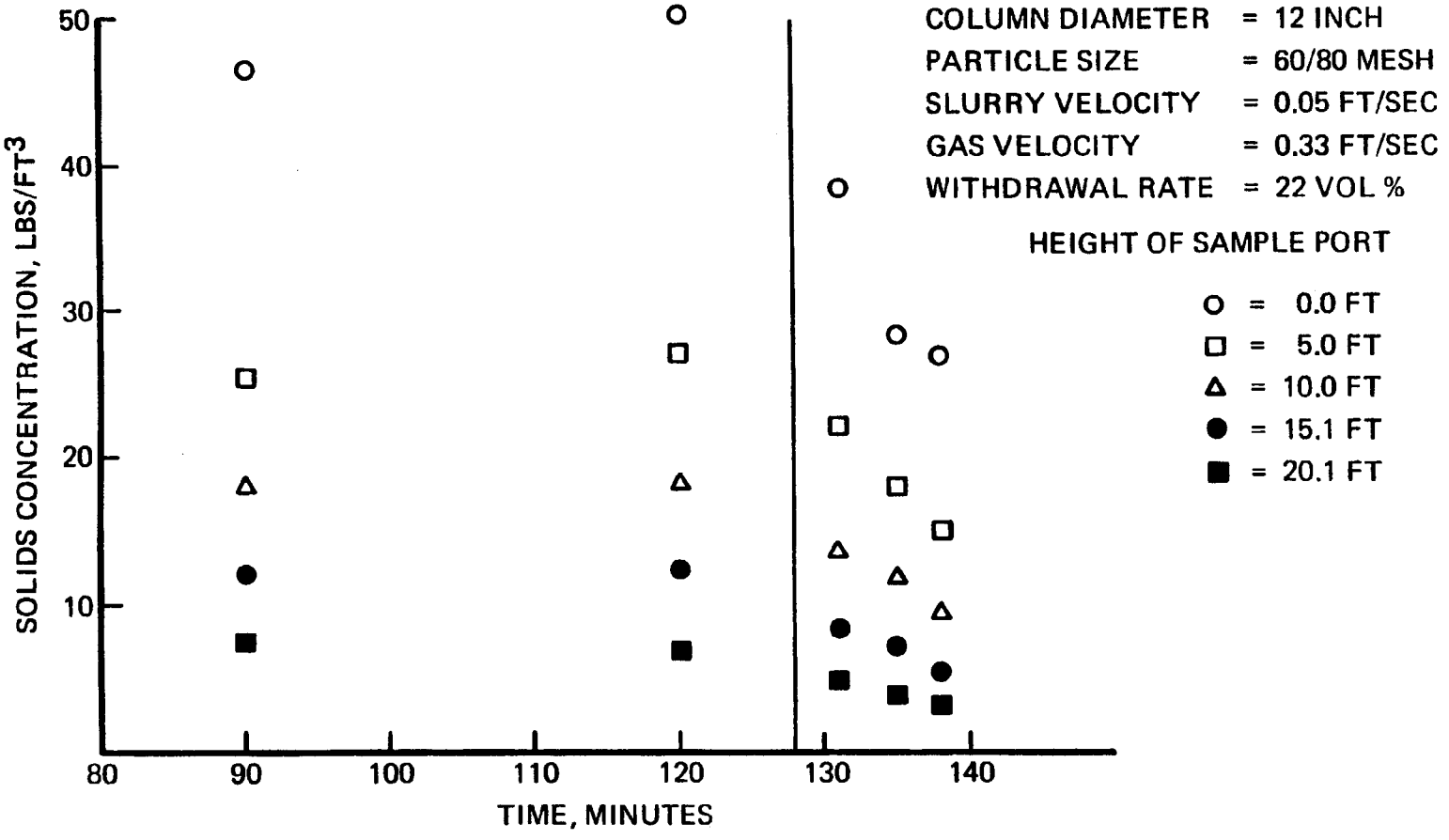

Figure 132. **EFFECT OF SOLIDS WITHDRAWAL ON AXIAL SOLIDS DISTRIBUTION**

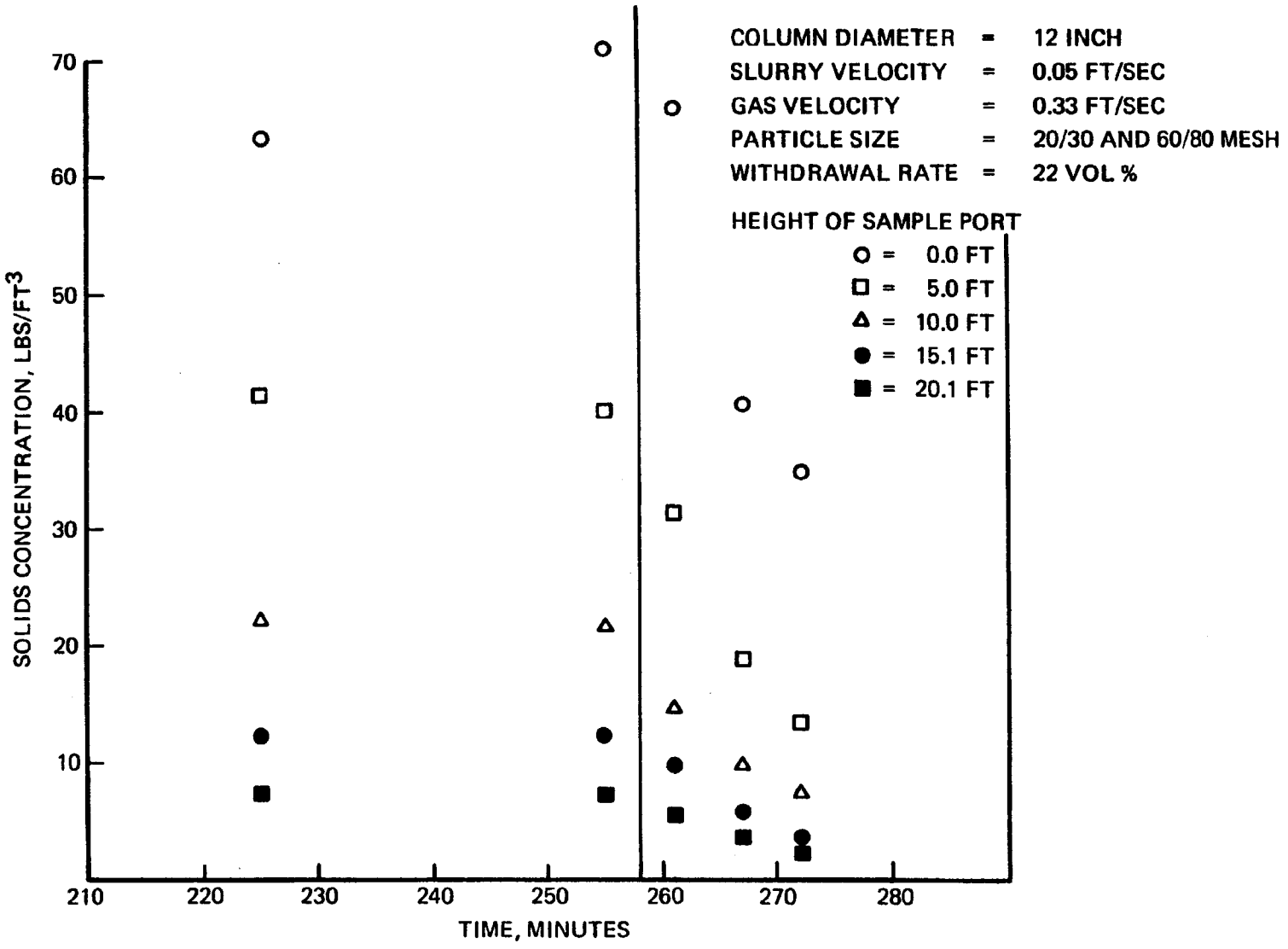

Figure 133

EFFECT OF SOLIDS WITHDRAWAL ON AXIAL SOLIDS DISTRIBUTION (IN THE PRESENCE OF LARGE & FINE PARTICLES)

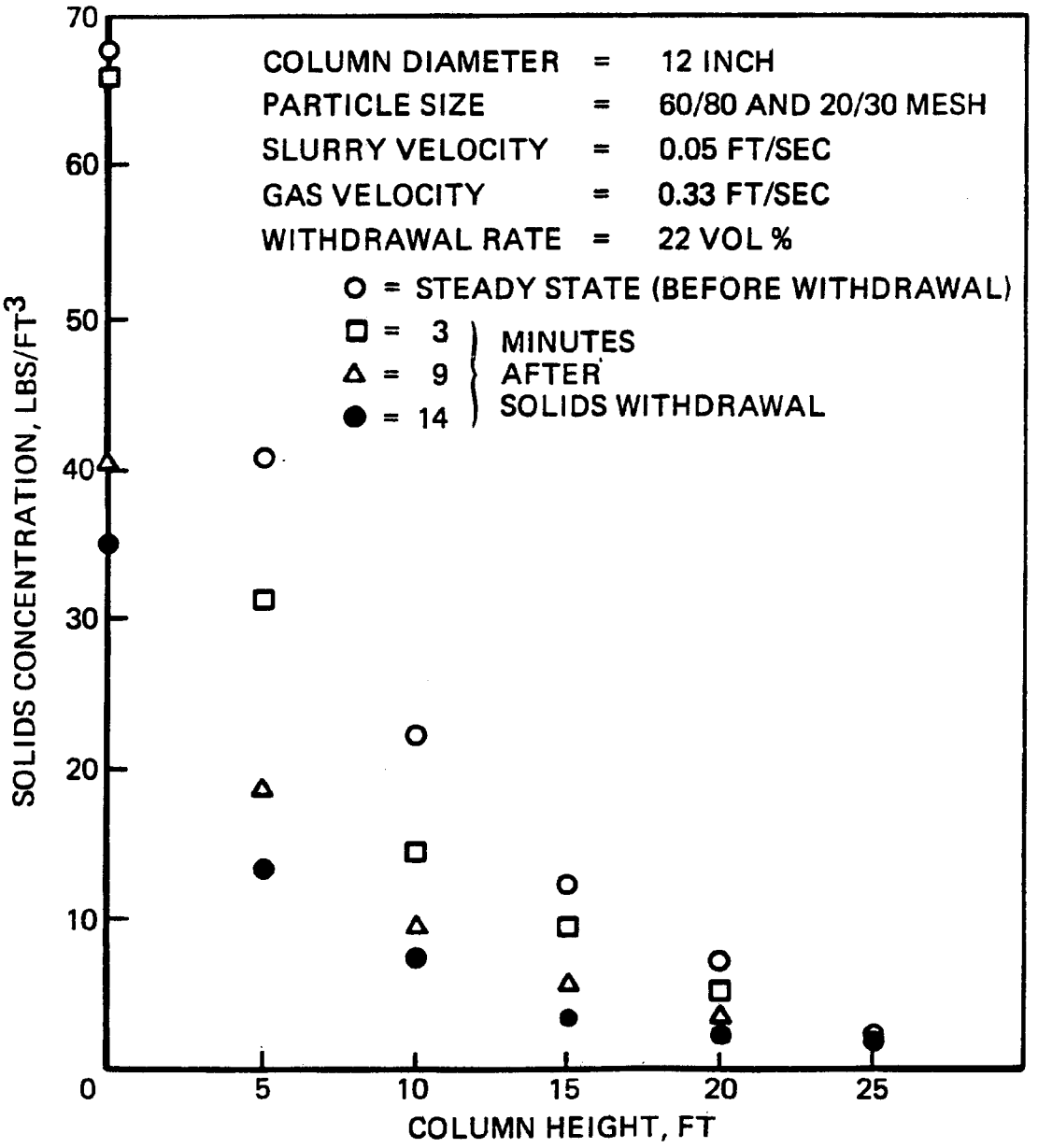

In addition, solids withdrawal from the bottom of the column depletes larger particles more quickly than small particles. In the experiment that used both 20/30 and 60/80 mesh particles, each sample was also screened to determine concentrations of individual particle sizes. Figure 134 illustrates the solid concentration profile of the individual particles before and 14 min. after the start of withdrawal. This figure clearly illustrates that the concentration of 20/30 mesh particles drops off more rapidly than that of 60/80 mesh particles.

When the column was drained at the end of the experiment, only 0.5 lb of the 88 lb that were retained in the column consisted of large particles. Table 33 which lists the variations in the composition of the withdrawal stream as a function of time, clearly indicates that large particles were drained first. As soon as solids removal started, the concentration of large particles in the withdrawal stream was quite large; this gradually decreased as the concentration of smaller particles increased.

Our results indicate that solids withdrawal can reduce solids accumulation and significantly change the axial solids concentration profile. Our data also indicate that larger particles are removed faster because they settle to the bottom more quickly. However, these results were obtained under non-steady-state operation and should be viewed with caution. Because of time restraints, this entire task was allotted only one month. Undoubtedly, steady-state experiments are needed in the future to determine the optimal withdrawal rate.

5.6 Particle/Particle Interaction

All of our solid distribution experiments were conducted with a narrow range of particle sizes. Individual experiments were conducted for large and small particles. In this section, we discuss results from a special set of experiments to shed some light on the effect of settled particles and particle/particle interactions on solids accumulation in the 12-in. diameter column.

Figure 134

EFFECT OF THE PRESENCE OF LARGE PARTICLES ON SOLIDS REMOVAL

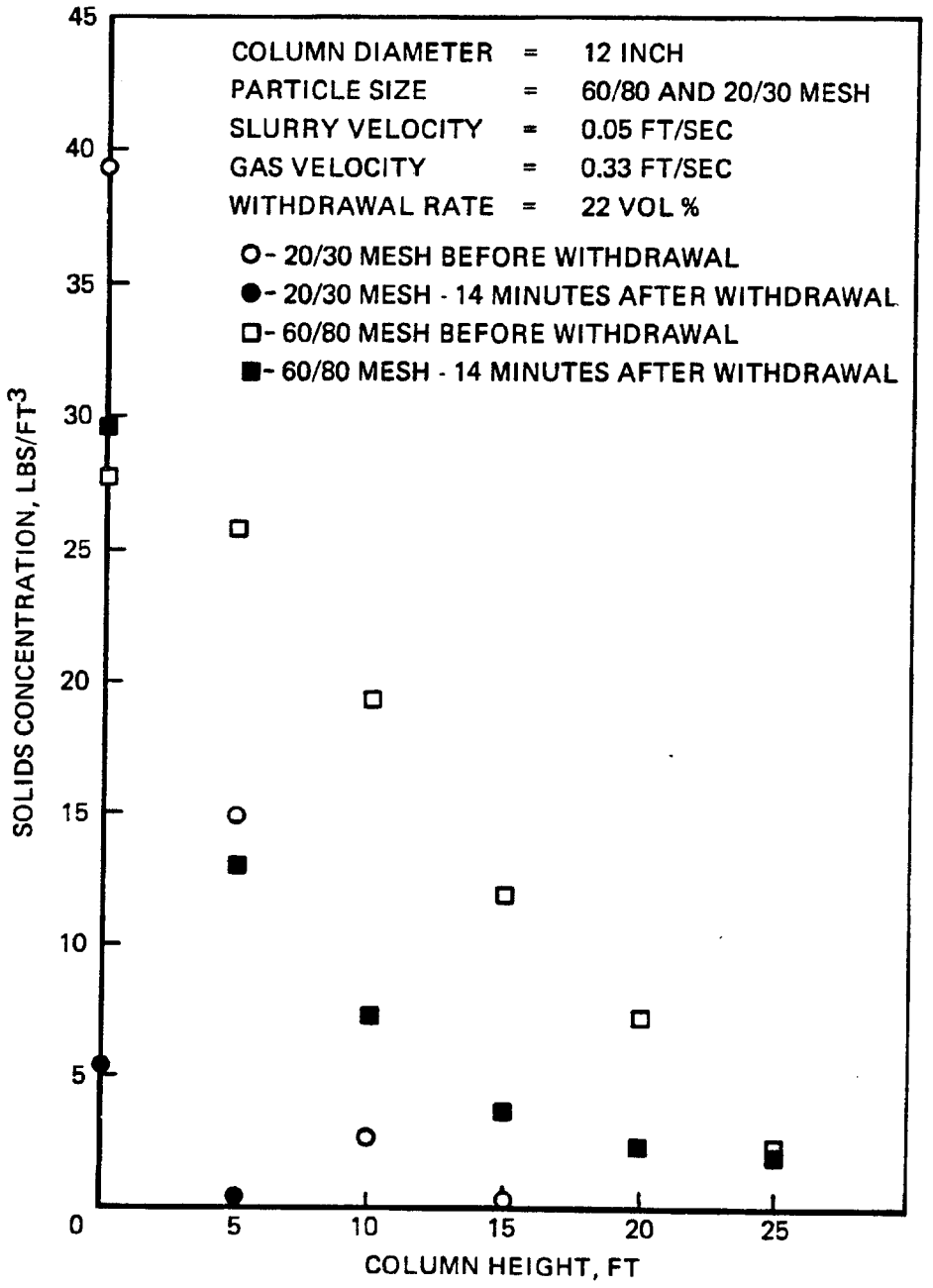

Table 33

Variations in the Composition of the Withdrawal Stream

	Time after start of solids removal (min.)		
	3	9	14
Total solids concentration (lb/ft^3)	79.7	85.6	68.9
Concentration of 60/80 mesh (lb/ft^3)	33.8	50.7	57.6
Concentration of 20/30 mesh (lbs/ft^3)	45.9	34.9	11.3

The experiments were detailed in the section on experimental procedure. Briefly, they consisted of three parts: (I) only -140 mesh sand was allowed to circulate through the column; (II) a mixture of 60/80 and -140 mesh sand was used to determine the effect of large but suspended particles on the accumulation of fines; (III) 20/30 mesh particles were placed in the column to simulate settled solids, and a slurry of 60/80 and -140 mesh sand was recycled through the column. Samples from parts II and III were screened to obtain the particle-size distribution.

The results show that the presence of large suspended particles does not influence the accumulation or distribution of fine particles. The settled particles also do not affect the distribution of either large suspended or fine particles. Figure 135 summarizes the results from all three parts of the experiment. Samples from parts II and III were screened to -100 mesh, 60/100 or 40/100 and +40 mesh particles. This procedure was adapted so that the samples could be screened more efficiently. Figure 135 plots the solids concentration as a function of column height for the three groups of particles. For simplicity, the particle sizes were distinguished as follows: +40 mesh particles are large, 60/100 or -40/100 mesh particles are medium; and -100 mesh particles are as small. The plot reveals that the presence of large particles does not affect the distribution of medium and small particles; the concentration profiles for particles from parts II and III are similar. For small particles, profile for part I does not fall in the same range as those for parts II and III, which show more fines. This small difference may be due to particle attrition from the medium particles, which were used extensively in this research program. Also note that the experiments in parts II and III classified -100 mesh particles as small, whereas -140 mesh particles were classified as small in part I. Some of the 60/80 mesh particles used in parts II and III could have contained smaller particles, increasing the concentration of small particles (Figure 135). In spite of the slight difference just mentioned, our results show that large particles have a negligible influence on the accumulation of fines. This discovery also implies that superimposing the concentration profiles of individual particle sizes to simulate a solids concentration profile for a wide range of particle sizes is valid.

Figure 135

PARTICLE–PARTICLE INTERACTION